Pitting Corrosion of Thermally Aged Duplex Stainless Steels at Different Temperature for Long Time

Yongqiang Wang[a], Hao Sun[a], Junliang Li[a], Dandan Li[a], Na Li[b]*

[a] *School of Materials Science and Engineering, Anhui University of Technology, Maanshan, China;*
[b] *School of Metallurgical Engineering, Anhui University of Technology, Maanshan, China*

The pitting corrosion of three duplex steels (DSS), SAF2205, SAF2507, Z3CN20.09M thermally aged at 350 - 500 °C for 5500 h was investigated by the means of electrochemical techniques. The pitting potential (E_p) of thermally aged Z3CN20.09M specimens decreased with increasing of ageing temperature, however, the E_p of SAF2205 and SAF2507 thermally aged specimens decreased first and reached the lowest value at 450 °C and then increased slightly. The electrochemical impedance spectroscopy results are coincident with the potentiodynamic polarisation testing results. The variation in the charge transfer resistance of specimens coincided with the E_p values. There is little influence of low temperature (below 350 °C) on resistance to pitting of SAF2205 and SAF2507 DSS. But, the pitting resistance of them degrades drastically ageing at higher temperature above 450 °C. The deterioration in pitting resistance of thermally aged DSS specimens mainly attributes to the precipitation of Cr-rich α′ phases which affected by temperature markedly. At the range of 350 -500 °C, the temperature the higher, the precipitation of Cr-rich α′ phases the more. The formation of G phases and the healing process during the long thermal ageing at 500 °C is the other reasons for the change in pitting resistance.

Keywords: *Duplex stainless steel, thermal ageing temperature, pitting corrosion, α′ phase, healing.*

1. Introduction

Duplex stainless steels (DSSs), which are characterized by austenite-ferrite dual microstructure, are widely used in many applications such as oil, petrochemical, marine and nuclear power industries due to their outstanding corrosion resistance, higher resistance to stress corrosion cracking and excellent mechanical properties[1-6]. However, they will be subjected to thermal aging embrittlement and sensitization when they are exposed to the temperature range of 320 -1000 °C mainly due to the formation of several undesirable precipitates such as α′, G, $M_{23}C_6$, σ, χ, etc in ferrite phase[2,7-10]. These precipitated phases not only severely decrease the toughness of steels but also negatively impact corrosion resistance, especially localised corrosion[11-13].

Pitting corrosion, the localized dissolution of a passivated metal in the presence of a solution of certain anionic species, is a major cause of failure of stainless steels owing to pits perforation or acting as an initiation site for cracking[14]. Generally, any factor whose can bring the defects in passive film or cause chemical or physical heterogeneity at the surface, such as inclusions, second phase particles, solute-segregated grain boundaries, flaws, mechanical damage, or dislocations, will be considered as the possible reasons for pitting corrosion[4,15-19]. Thermal aging embrittlement induced by the spinodal decomposition of ferrite phases into coherent Cr-enriched α′ and the precipitation of G-phase in ferrite can also degrade the pitting resistance of DSS. In the past decades, many works have been done to investigate the localized corrosion behaviors of thermally aged DSS. Some of them reported the mechanism of the effect of thermal aging on pitting corrosion or intergranular corrosion[12,20]. In others, the researches on the chemical or electrochemical of thermally aged DSS only were used to evaluate the material degradation induced by thermal aging[21,22]. However, on one hand, a few attempts have been taken to discuss the effect of different thermal aging temperature on the pitting resistance of them, especially for the DSS thermally aged for a long time. Temperature is one of the most important factors for the thermal aging embrittlement of DSS and can certainly affect the pitting corrosion. On the other hand, duplex stainless steels which used for the primary coolant pipe of nuclear power plants are long-term serviced at the high temperature and pressure water containing Cl^-, Li^+ and BO_3^{3-} environment that could cause thermal aging embrittlement and corrosion of pipe. Localised corrosion is one of the most main breakages of primary coolant pipe[23]. The research on the effect of temperature on the pitting corrosion of thermally aged DSS is helpful for the evaluation of safety working of nuclear power plant.

The aim of this work is to examine the effect of thermal aging temperature on the pitting corrosion of duplex stainless steel. Three SAF2205, SAF2507 and Z3CN20.09M DSS are adopted to make efforts to elucidate the mechanism of the effect of temperature on pitting corrosion conveniently. Pitting behaviors of thermally aged specimens were investigated by using potentiodynamic polarisation and electrochemical impedance spectroscopy technologies. There are differences in chemical composition and microstructure between SAF2205, SAF2507 and Z3CN20.09M DSS. The investigation was performed after thermal aging at 350 -500 °C temperatures

*e-mail: linaustb@163.com

for 5500 h. The investigation results of different DSS can more convincing.

2. Experimental Details

2.1 Materials

The chemical compositions of the studied three duplex stainless steels, SAF2205, SAF2507 and Z3CN20.09M are listed in Table 1. These DSSs were annealed at 1050 °C, 1100 °C, 1180 °C for 0.5 h, respectively, for solid solution first followed by water quenching. And then, they were thermally aged for 5500 h at the temperature 350 °C, 450 °C, 500 °C respectively. The different size specimens cut from the thermally aged DSS samples were used to the microstructure examination, microhardness measurement and pitting corrosion investigation.

2.2 Microstructures examination and microhardness measurement

The DSS specimens with a size of 10 mm×10 mm× 10 mm are used for the microstructure examination and microhardness measurement. The specimens were abraded using silicon carbide abrasive paper to 2000# and then polished by diamond paste with a size of 1.5 μm. Finally, the specimens were electrochemically etched for 10-20 s in a 20 wt% NaOH solution in distilled water with a direct voltage of 3 V in order to differentiate the ferrite, austenite or other phases. The microstructures of the specimens were observed by optical microscopy (OM) and transmission electron microscopy (TEM). The ferrite content in specimens was calculated on 20 optical measurements for each specimen by using quantitative metallography analysis software (Image-Pro Plus6.0). The microhardness of ferrite and austenite phases in the DSS specimens was measured with a WOLPERT 401MVD microhardness instrument.

2.3 Electrochemical measurements

DC electrochemical measurements were performed with a CHI electrochemical workstation (CH Instruments). The three DSS specimens with a size of 10 mm ×10 mm× 3 mm are used as working electrodes. They were prepared by spot welding a copper wire onto one side of each specimen and then embedded in epoxy resin with an exposure area of 1 cm^2. The reference electrode is a saturated calomel electrode (SCE) and a Pt foil is used as the auxiliary electrode.

Pitting corrosion tests were carried out in a 0.5 mol/L NaCl solution at constant temperature (30±1 °C) by potentiodynamic anodic polarization and electrochemical impedance spectroscopy (EIS) techniques to evaluate the pitting potential (E_p) and the passive layer breakdown of the specimens, respectively. E_p is defined as the potential at which the current increases sharply from the passive current level[14]

Before testing, the working electrodes were immersed in the test solution for 30 min until the steady-state open circuit potential (E_{ocp}) was reached. In addition, a potential sweep was applied in the anodic direction at a scan rate of 20 mV/min from -400 mV (SCE) to an appropriate value. EIS measurements were carried out using the frequency range of 100 kHz to 0.01 Hz at the E_{ocp}. Amplitudes of all sinusoids were equal to 10 mV rms. The EIS results were interpreted using an equivalent circuit. The characteristic parameter values of these elements in an equivalent circuit were then obtained directly by fitting the experimental curves using the Zview Version 3.1® software.

3. Results and Discussions

3.1 Microstructures of thermally aged DSS specimens

Figure 1 shows the microstructures of solid solution and thermally aged SAF2205, SAF2507, Z3CN20.09M specimens, which consist of austenite (gray) and ferrite (dark) phases. No other phase is apparently observed in these specimens aged at the temperature range of 350 - 450 °C. Moreover, the volume fraction of ferrite phase in thermally aged specimens is almost equal to that of solid solution ones (seen in Figure 2). Thermal aging embrittlement of DSS are mainly induced by the formation of α' phase by ferrite spinodal decomposition and the precipitation of G-phase in ferrite. These precipitates are very small, moreover, α' phase is coherent or semi-coherent with ferrite matrix[10]. On the other hand, the other transformations, for instance, σ, χ precipitation or α → γ don't happen at the temperature range of 350 °C to 500 °C according to the thermodynamics of phase transition and phase diagrams of the three DSS[2]. So, there is hardly any influence of thermal ageing on ferrite content, size and morphology. However, some precipitates can be found in the aged SAF2205, SAF2507 specimens at 500 °C (Figure 1d) and a few carbide $M_{23}C_6$ can form in the aged Z3CN20.09M specimen at

Table 1. Chemical compositions of three duplex stainless steels (wt.%)

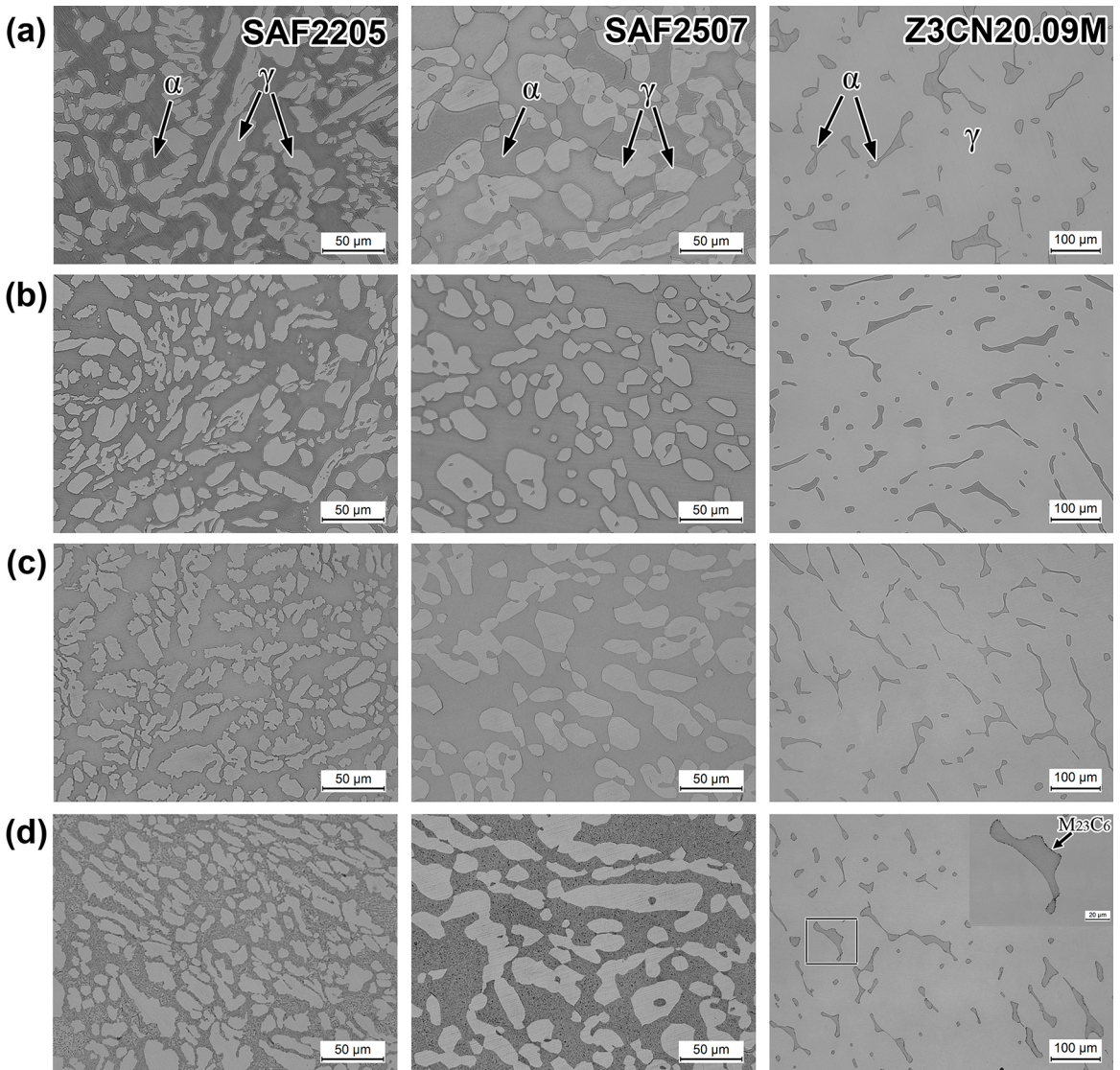| Type	Elements(wt%)									
	C	Si	Mn	P	S	Cr	Ni	Mo	N	Fe
SAF2205	0.023	0.380	1.35	0.026	0.001	22.07	4.83	2.37	0.190	balance
SAF2507	0.023	0.497	1.55	0.020	0.001	25.15	7.37	4.35	0.250	balance
Z3CN20.09M	0.027	1.270	1.13	0.023	0.0009	20.19	8.92	0.21	0.031	balance

Figure 1. Microstructures of DSS specimens solid solution (a) and thermally aged for 5500h at different temperature (b) 350℃, (c) 450℃, (d) 500℃
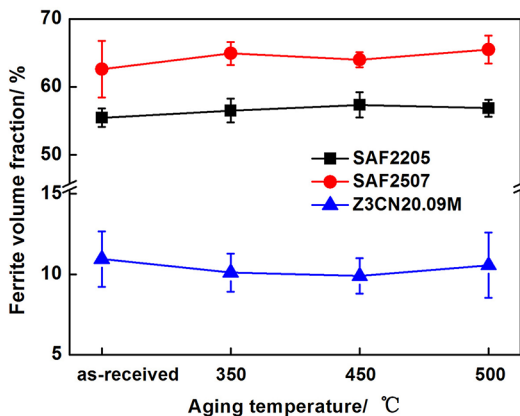

Figure 2. Ferrite volume fraction of specimens thermally aged at different temperature

500 ℃ on the basis of phase diagram calculated using Thermo–Calc software [9].

In order to detect the changes in microstructures of ferrite in thermally aged DSS specimens, the microstructures after thermal ageing were examined by Transmission Electron Microscopy (TEM). Figure 3a and b show the bright-field TEM images of Z3CN20.09M specimens thermally aged at 450 ℃ and 500 ℃ respectively. The mottled contrast in the ferrite phase could clearly be observed in the specimen aged at 450 ℃ (Figure 3a). Small particles of α′ phases and G phases of a few nanometer in size are visible in ferrite phase of the specimens aged at 500 ℃ (Figure 3b). The mottled contrast in the ferrite phase has been attributed to the compositional

fluctuation induced by spinodal decomposition of ferrite phase into Fe-rich α and Cr-rich α′ [24]. The observation performed on Z3CN20.09M DSS aged at 500 °C indicates that in this specimen condition α → α + α′ phase separation takes place via a nucleation and growth mechanism[25]. Similar microstructures were observed for other thermally aged specimens (SAF 2205 and SAF2507) at 450 °C and 500 °C indicating that spinodal decomposition of ferrite in the three DSS takes place at below temperatures 500 °C. Nevertheless, α′ phases precipitate in ferrite of thermally aged DSS specimens at 500 °C by nucleation and growth.

3.2 Microhardness of thermally aged DSS specimens at different temperature

Figure 4 displays the microhardness of different DSS specimens. One can see that there is no change in the microhardness of austenite phase with ageing period and there is little scattering in the hardness values. However, the ferrite hardness is found to change substantially with ageing time. With increasing thermal ageing temperature the hardness of ferrite phase increased first and reached the highest value at 450 °C and then decreased. Based on these results, the increase in the hardness of ferrite phase can be used to represent the degree of embrittlement in thermally aged DSS, although, it cannot exactly represent the overall embrittlement of the material because of the other effects, e.g., ferrite fraction and its distribution[24]. However, it reflects the embrittlement of the ferrite phase directly only

which is the main cause of embrittlement observed in the material. The hardness results of ferrite indicate that the most serious thermal ageing embrittlement of all the three DSS specimens has taken place at temperature 450 °C. Comparing with 450 °C, the decrease in hardness of ferrite in specimens aged at 500 °C might mainly attribute to the formation of α′ phase via nucleation and growth but not by spinodal decomposition of ferrite. Similar to the present result of hardness variation with ageing temperature was also reported by Mats Hättestrand et al[25]. The other possible reason is the healing or desensitisation phenomenon occurring in the ferrite phase, whereby, the Cr diffusion reduces or completely eliminates the concentration gradient of Cr[26,27]. Both of these above processes can cause the reduction of interface stress of α′ and α phase.

3.3 Potentiodynamic anodic polarisation curves of thermally aged DSS specimens

Figure 5 shows the polarisation curves of different SAF2205, SAF2507, Z3CN20.09M specimens. Based on the polarisation curves, the variation in pitting potential (E_p) for the different specimens can be found, as shown in Figure 6. One can see that the E_p of the solid solution SAF2507 specimen is the highest, while the E_p of the solid solution Z3CN20.09M specimen is the lowest. Besides, the E_p of aged Z3CN20.09M specimen became less positive than that of solid solution ones and decreased with the increase of thermal ageing temperature. However, the E_p of aged SAF2205 and
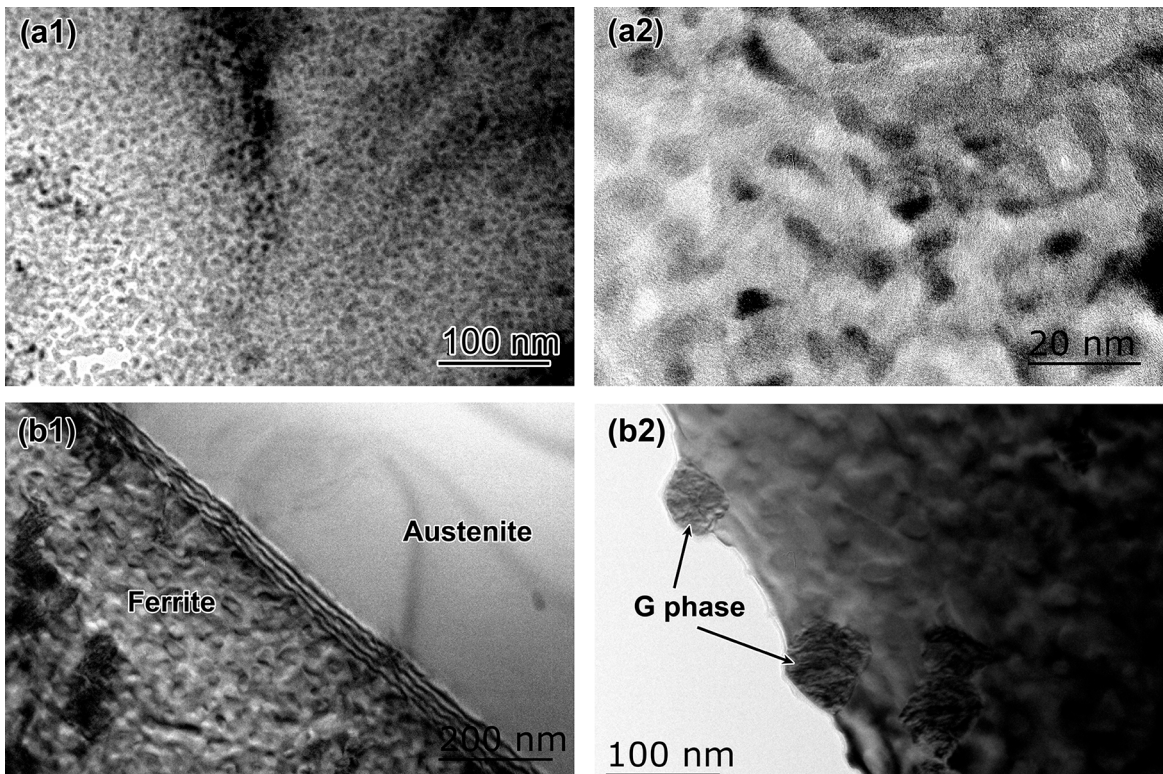

Figure 3. Bright-field TEM micrographs for Z3CN20.09M DSS specimens aged at different temperature (a) 450 °C and (b) 500 °C
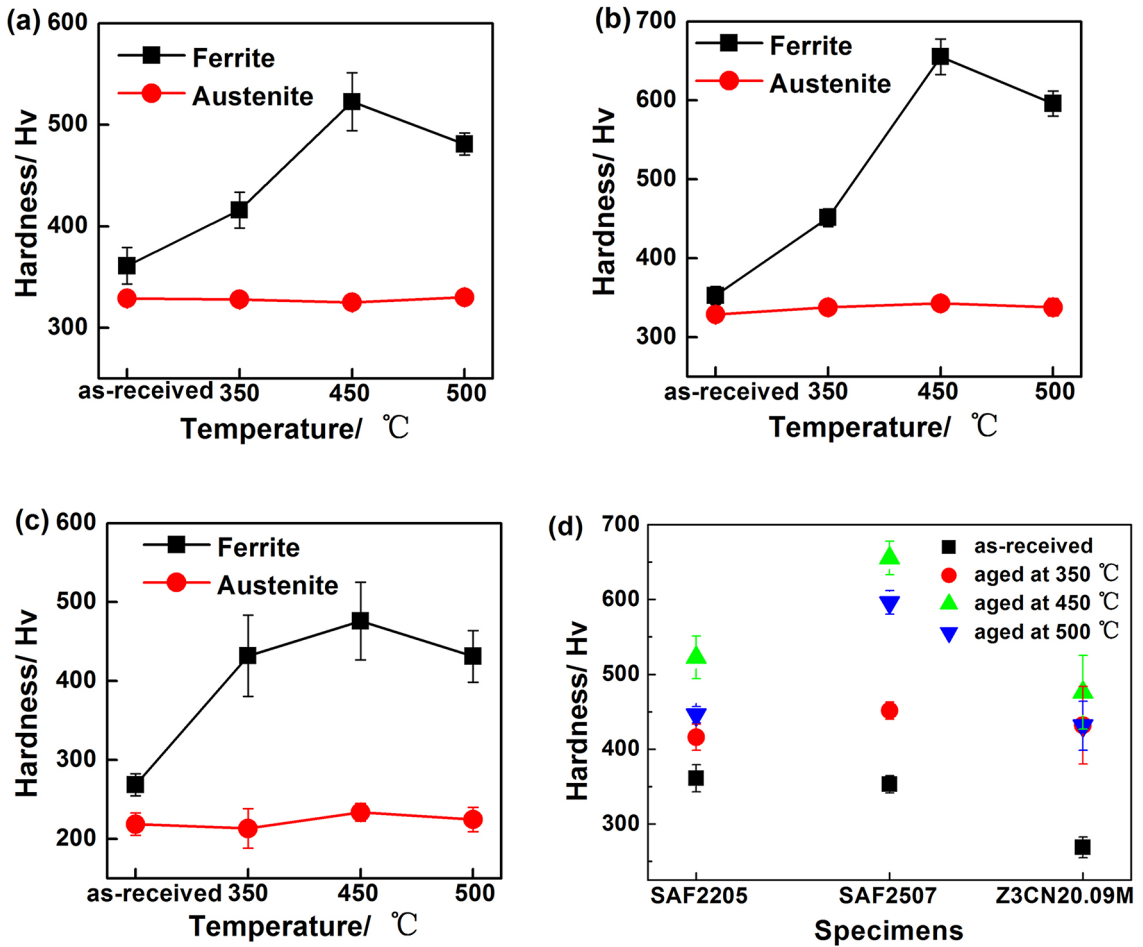
Figure 4. The changes in microhardness of three thermally aged DSS specimens with thermal ageing temperature (a) SAF2205, (b) SAF2507, (c) Z3CN20.09M and (d) hardness of ferrite in different thermally aged DSS specimens

SAF2507 specimens decreased firstly and then increased slightly with thermal ageing temperature (Figure 6a). The lowest E_p was found in SAF2205 and SAF2507 specimens thermally aged at 450 °C. Moreover, the E_p of Z3CN20.09M specimen aged at 450 °C and 500 °C is higher than that of the SAF2205 and SAF2507 specimens aged at the same temperature. Among the three DSS specimens thermally aged at 500 °C, The E_p of SAF2507 specimen is the lowest (Figure 6b). The micrographics of different Z3CN20.09M specimens after the electrochemical tests are shown in Figure 7. The number of pits in specimens increased with ageing temperature. Moreover, the morphology of pits is different significantly. The pits in the solid solution specimen formed at the interface of ferrite/austenite boundary frequently (Figure7a). However, abundant pits were found in the ferrite phase in thermally aged specimens especially in ones aged at 500 °C (Figure7d).

Thermal ageing induces the precipitation of Cr-rich α′ phases in ferrite and brings the Cr-depleted zones around them. The interface between Cr-enriched α′ phase and Cr-depleted zone could become the preferential sites for pits initiation, subsequently, pits grew in ferrite[13,28,29]. The more

the precipitation of α′ phases and Cr-depleted zones, the worse the pitting resistance of DSS specimens revealing by the lower E_p value. Thermal ageing embrittlement of stainless steel is mainly decided by ageing time, ageing temperature, chemical composition and ferrite phase fraction. At certain range of temperature, on the one hand, the higher the thermal ageing temperature, the more the Cr-enrich α′ phase. On the other hand, the higher the Cr element content and the more the ferrite phase fraction, the more the precipitation of Cr-enrich α′ phase and Cr-depleted zone. So the E_p value of the three DSS specimens decreased with increasing of thermal ageing temperature until 450 °C. Meanwhile, the E_p of aged SAF2507 specimen is lower than that of SAF2205 and Z3CN20.09M specimens at the same ageing temperature, for instance 450 °C and 500 °C, due to the highest Cr content and the most ferrite phase in SAF2507 DSS. It is worth noting that the smooth increase in E_p of SAF2205 and SAF2507 specimens aged at 500 °C is maybe due to a healing or desensitization process[26,27], which is caused by the chromium diffusion reducing or eliminating the gradient of concentration of this element and the interface of Cr-enrich α′ phase and Cr-depleted zones. The decrease
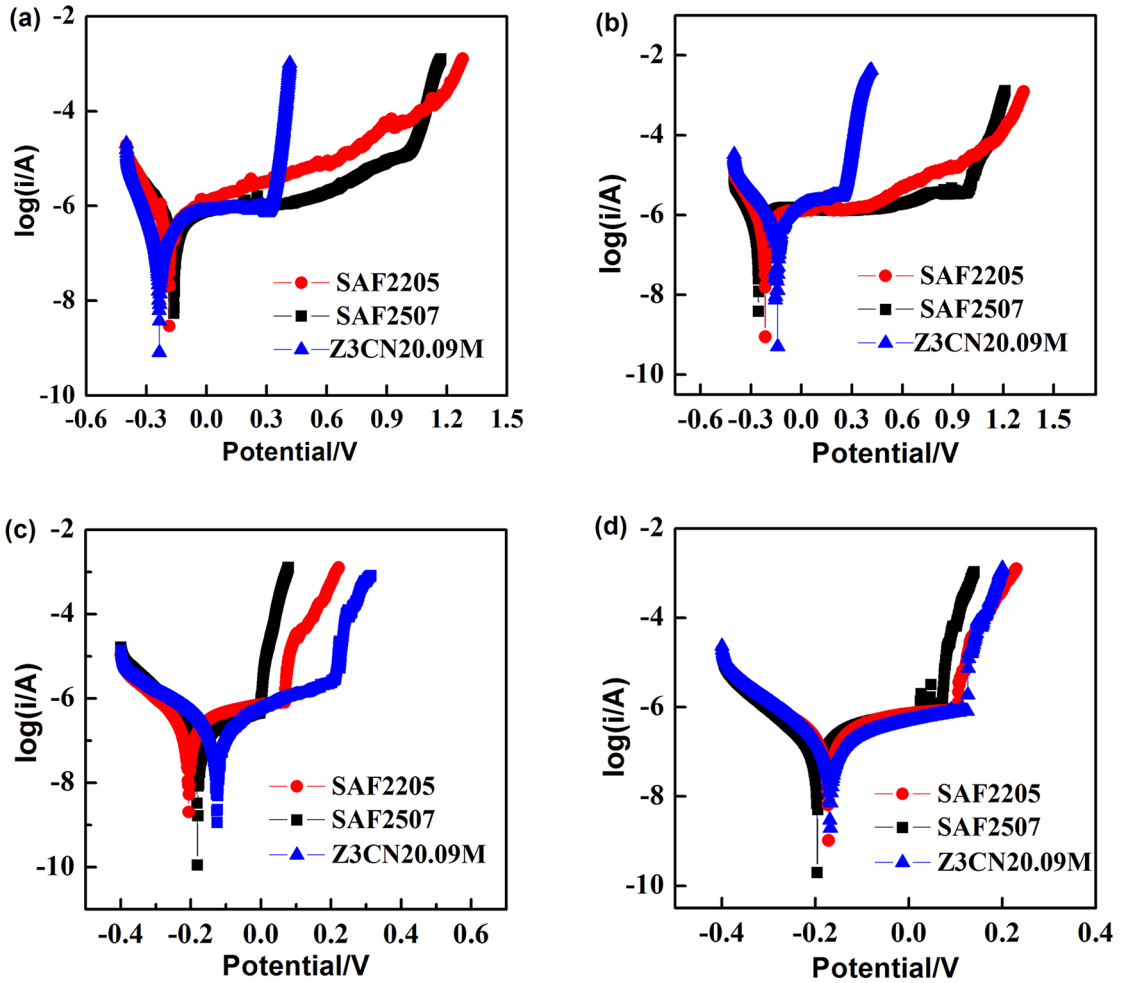
Figure 5. Polarisation curves of DSS specimens aged at different temperature (a) solid solution, (b) 350℃, (c) 450℃, (d) 500℃
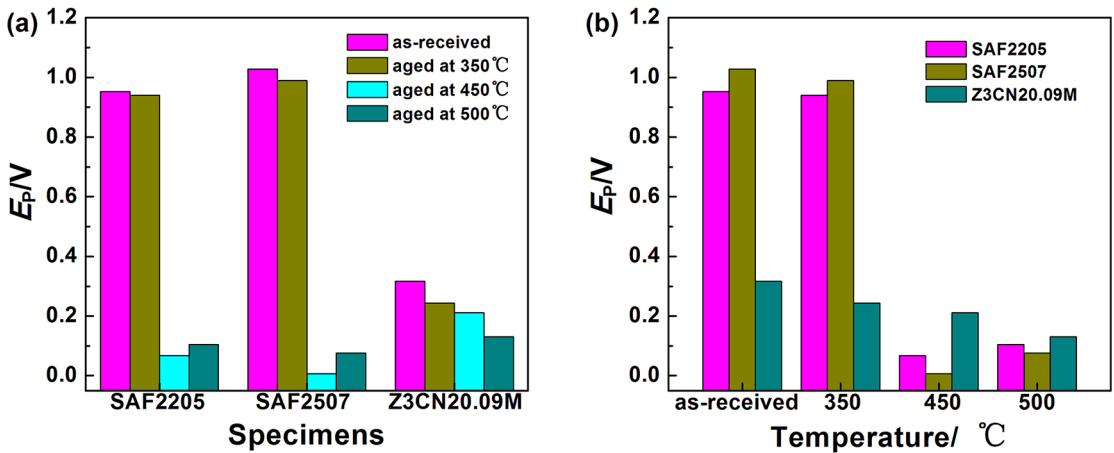

Figure 6. Pitting potential of (a) different thermally aged DSS specimens and (b) different thermal aging temperature
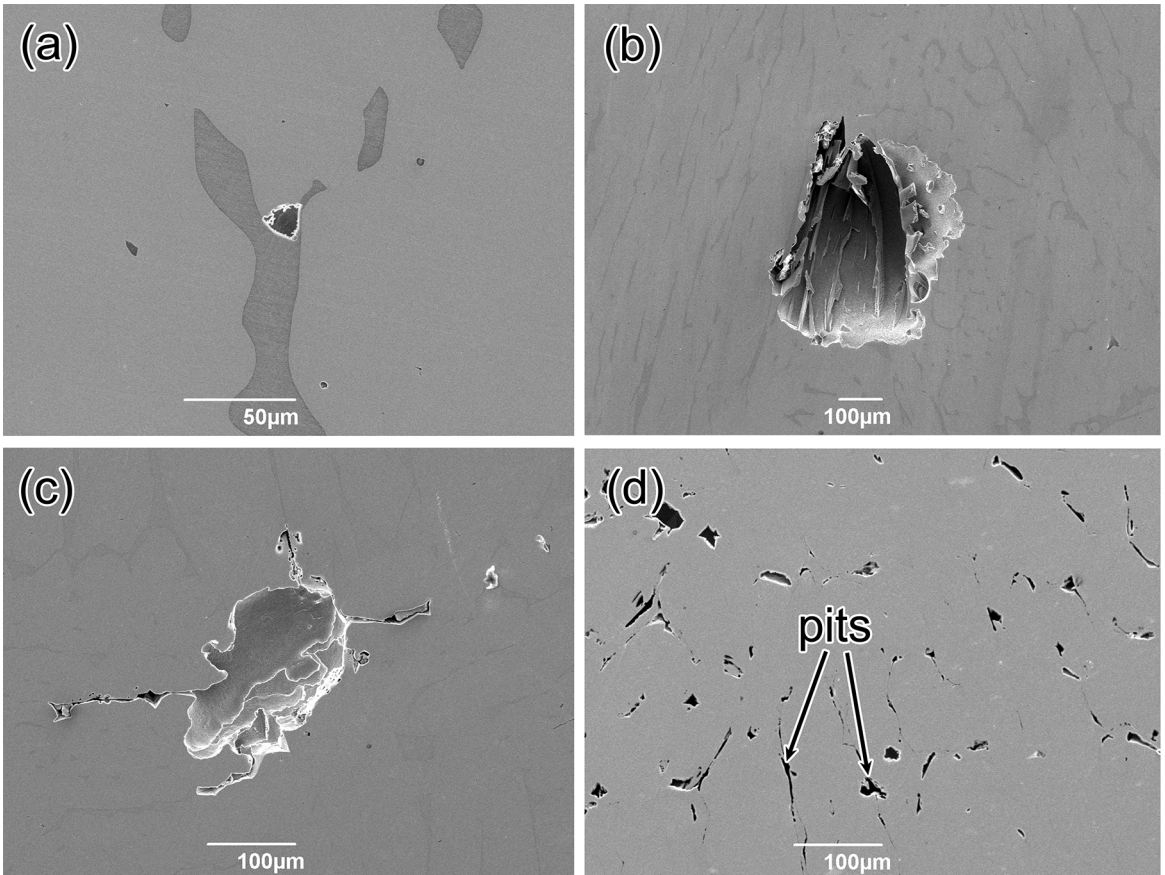
Figure 7. The micrographics of different Z3CN20.09M specimens after the electrochemical tests (a) solid solution, (b) 350℃, (c) 450℃, (d) 500℃

in E_p of Z3CN20.09M specimens aged at 500 ℃ should be ascribed to the formation of considerable G phases in ferrite and few $M_{23}C_6$ carbides on the α/γ boundary.

3.4 EIS results of thermally aged DSS specimens

Figure 8 shows the EIS results of specimens thermally aged at different temperature and different DSS specimens. The distinct differences of semicircle arcs for different specimens existing in the Nyqusit plots can be found in the figure. In general, the decrease in the semicircle arc radius is indicated by the decrease in the charge transfer resistance (R_{ct}) value which is inversely proportional to the corrosion rate of the system. The semicircle arc radius of Z3CN20.09M specimen decreased with thermal ageing temperature. It means that electric charges in these specimens aged at high temperature transfer easily through the passive film of specimens. However, the semicircle arc radius of SAF2205 and SAF2507 specimens decreased first and then increased with thermal aging temperature. The lowest values of semicircle arc radius were found in these specimens aged at 450 ℃.

An equivalent electrical circuit was designed as a best-fit to the EIS experimental results and is displayed in Figure 9, which consists of the arrangement of $[R_s(\text{CPE} \| R_{ct})]$ elements, where R_s is the solution resistance and CPE is the constant phase in parallel connection with R_{ct} which is the charge transfer resistance at the interface. All the fitting parameters of the impedance plots are shown in Table 2. From the table, the R_{ct} value of Z3CN20.09M specimen decreased with the increase of thermal ageing temperature and reached the lowest value at 500 ℃. While, the R_{ct} of SAF2205 and SAF2507 specimens decreased first and then increased slightly with thermal ageing temperature, and reached the lowest value in these specimens aged at 450 ℃. Moreover, the R_{ct} value of SAF2507 specimens thermally aged at 350 ℃ is the highest among the three DSS specimens. However, the R_{ct} values of SAF2507 specimens thermally aged at 450 ℃ and 500 ℃ are both lower than those of SAF2205 and Z3CN20.09M specimens.

The precipitation of Cr-rich α′ phase induced by the thermal ageing embrittlement brings the segregation of Cr element that is one of the most important factors for the passive film on the surface of stainless steels. The segregation of Cr element makes passive film less protective. The more serious the thermal ageing, the greater the segregation of Cr element, therefore, the worse the pitting resistance is. Because the most serious thermal ageing embrittlement occurs in the SAF2507 specimens thermally aged at 450 ℃ due to the highest Cr content, the most ferrite fraction and higher temperature, so the worst pitting resistance was performed
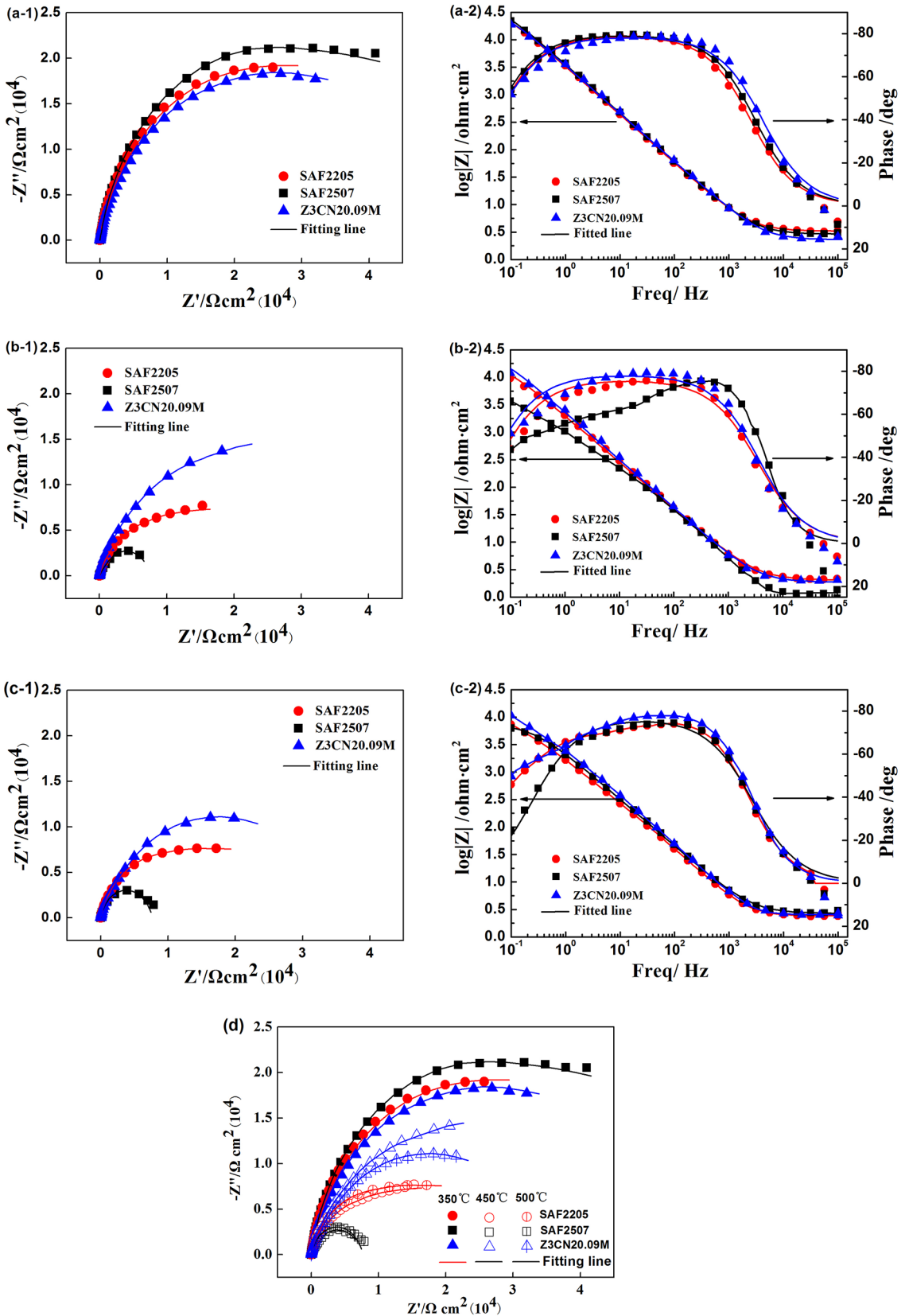
Figure 8. Nyqusit plots for specimens thermally aged at different temperature (a) 350℃, (b) 450℃, (c) 500℃ and (d) different DSS specimens
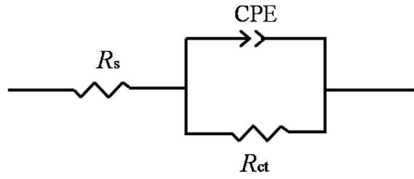
Figure 9. Equivalent circuit for fitting experimental Nyquist impedance plots

revealing by the lowest R_{ct} value, as shown in Table 2. The increase in R_{ct} of SAF2205 and SAF2507 specimens thermally aged at 500 °C should be attributed to the healing which reduced or alleviated the segregation of Cr element.

3.5 Mechanism of the effect of thermal temperature on pitting

The corrosion resistance of stainless steels is closely related to the passive film on their surface, which is mainly determined by alloy composition, electrolyte media, and condition of the material[4,14]. Cr is the most important element in conferring passivity to stainless steels[4] and Mo is another very important element for improving the pitting resistance of stainless steels[30,31]. The pitting potential of stainless steels correspondingly becomes more positive remarkably, as Cr and Mo concentration increases[14,32]. Therefore, the highest E_p values that indicating the best pitting resistance are obtained in the solid solution SAF2507 specimens for the highest Cr and Mo content of them. The lowest E_p values are found in the solid solution Z3ZN20.09M specimens due to the fewest Cr and Mo element (Figure 5a, Figure 6b).

The condition of stainless steel has been changed when they are subjected to thermal ageing for long time. Thermal ageing brings the segregation of Cr due to the precipitation of Cr-rich α′ phases and the formation of Cr-depleted zones around α′ phases. So the resistance to pitting of DSS becomes poor with thermal ageing development. G phases also precipitate in ferrite during thermal ageing, especially for high ageing temperature and long ageing time. Although, G phases enriched in Ni and Si elements which are not sensitive to pitting corrosion will not obviously induce pitting

themselves[4,10], the pitting resistance of thermally aged DSS might be affected negatively by the precipitation of them due to the stress of G/α ferrite interface and the Cr depletion adjacent to the G-phase precipitates[12,24]. Considerable G phases precipitated in ferrite of Z3CN20.09M specimen aged at 500 °C due to higher Ni content, as shown in Figure 3. Thus, the E_p still decreased when ageing temperature increased to 500 °C although healing occurred in thermally aged Z3CN20.09M specimens too. Another reason for the decrease in E_p of the aged Z3CN20.09M specimen at 500 °C is some the precipitation of $M_{23}C_6$ carbide on the boundary of α/γ, as shown in Figure 1d[29].

Possible healing mechanisms for DSSs thermally aged in the spinodal decomposition temperature range are: 1. back diffusion of Cr atoms from α′ phase to Cr-depleted zone and 2. diffusion of Cr atoms from the austenite to Cr-depleted zone [33] . High temperature can make the back diffusion of Cr atoms effective. Healing is also directly related with the composition of DSS especially Cr content and ferrite phase fraction. High Cr content and ferrite fraction are propitious to improve the diffusion of Cr atoms that are not only in ferrite matrix but also austenite to Cr-depleted zone, so the effective healing was found in the thermally aged SAF2205 and SAF2507 specimens with higher Cr content and ferrite fraction at 500 °C revealing by the increase of E_p. For the ineffective healing occurring in the Z3CN20.09M specimens due to the less ferrite phase and low Cr content did not bring positively influence on pitting resistance enough, hence, the decrease in E_p of these specimens aged at 500 °C was still achieved.

4. Conclusions

(1) Pitting corrosion of SAF2205, SAF2507 and Z3CN20.09M duplex stainless steels is affected by thermal ageing temperature. The pitting potential of Z3CN20.09M DSS specimens became less positive with the increase of thermal ageing temperature from 350 °C to 500 °C. While, the E_p values of thermally aged SAF2205 and SAF2507 specimens decreased first and reached the lowest level at 450

Table 2. EIS-fitted values of three DSS specimens in 0.5 mol L^{-1} NaCl solution.

Thermal ageing temperature/°C	Specimen	R_s	CPE-T/Fcm^2	CPE-n	R_{ct}
350	SAF2507	2.915	1.5715E-5	0.88786	50962
	SAF2205	3.294	1.6296E-5	0.88231	44501
	Z3CN20.09M	2.299	1.4894E-5	0.87936	40868
450	SAF2507	1.038	2.0828E-5	0.79139	6097
	SAF2205	2.227	1.9945E-5	0.82435	16973
	Z3CN20.09M	1.878	2.2600E-5	0.87976	26694
500	SAF2507	2.664	1.8811E-5	0.85555	7786
	SAF2205	2.040	2.0609E-5	0.85175	19445
	Z3CN20.09M	2.375	1.8056E-5	0.85509	24127

°C and then increased slightly with increasing ageing temperature.

(2) EIS results of three DSS specimens are coincident with the potentiodynamic polarisation testing results. The changes in the charge transfer resistance of SAF2205, SAF2507 and Z3CN20.09M specimens that affected by thermal ageing temperature are the same as the E_p values variation. It can be concluded that the resistance to pitting of Z3CN20.09M specimen thermally aged at 500 °C is the worst, however the worst happening of pitting corrosion is found in SAF2205 and SAF2507 specimens aged at 450 °C. There is little influence of low temperature (below 350 °C) on the resistance to pitting of SAF2205 and SAF2507 DSS. But, the pitting resistance of them degrades drastically ageing at higher temperature above 450 °C.

(3) The precipitation of Cr-rich α′ phases in ferrite and the formation of Cr-depleted zones around α′ phases induced by thermal ageing is the main reason for the deterioration in pitting corrosion. The higher the ageing temperature, the more the α′ phases and Cr-depleted zones, thus the pitting resistance of SAF2205, SAF2507 and Z3CN20.09M specimens became poor when they were thermally aged at from room temperature (unaged) to 450 °C. The further decrease in pitting potential of Z3CN20.09M specimens attributed to the precipitation of considerable G phases and a few $M_{23}C_6$ carbides.

(4) Pitting potential of SAF2205 and SAF2507 specimen thermally aged at 500 °C became little more positive than that of them thermally aged at 450 °C due to a healing or desensitization process, which is caused by the chromium diffusion reducing or eliminating the gradient of concentration of this element and the interface of Cr-enrich α′ phase and Cr-depleted zone. Although considerable G phase can form in the thermally aged SAF2205 and SAF2507 specimens at 500 °C too, the degradation of pitting corrosion resistance owing to the G phases does not enough to smooth the recovery of pitting resistance induced by the healing of thermal ageing.

5. Acknowledgments

6. References

1. Gunn RN. *Duplex Stainless Steels: microstructure, properties and applications*. Cambridge: Woodhead Publishing; 1997.

2. Lo KH, Shek CH, Lai JKL. Recent developments in stainless steels. *Materials Science and Engineering: R*. 2009;65(4-6):39-104.

3. Rovere CAD, Santos FS, Silva R, Souza CAC, Kuri SE. Influence of long-term low-temperature aging on the microhardness and corrosion properties of duplex stainless steel. *Corrosion Science*. 2013;68:84-90.

4. Olsson COA, Landolt D. Passive films on stainless steels-chemistry, structure and growth. *Electrochimica Acta*. 2003;48(9):1093-1104.

5. Wang YQ, Li N. Effect of ferrite on the precipitation of σ phase in cast austenitic stainless steel used for primary coolant pipes of nuclear power plants. *Materials Research*. 2017;20(6):1690-1696.

6. Tranchida G, Clesi M, Franco FD, Quarto FD, Santamaria M. Electronic properties and corrosion resistance of passive films on austenitic and duplex stainless steels. *Electrochimica Acta*. 2018;273:412-423.

7. Mathew MD, Lietzan LM, Murty KL, Shah VN. Low temperature aging embrittlement of CF-8 stainless steel. *Materials Science and Engineering: A*. 1999;269(1-2):186-196.

8. Sahu JK, Kruppc U, Ghosh RN, Christ HJ. Effect of 475 °C embrittlement on the mechanical properties of duplex stainless steel. *Materials Science and Engineering:A*. 2009;508(1-2):1-14.

9. Wang YQ, Han J, Yang B, Wu HC, Wang X. Precipitation behavior of the intermetallic phases in Z3CN20.09M stainless steel for primary coolant pipes of nuclear. *Acta Metallurgica Sinica*. 2013;49(4):415-420.

10. Li S, Wang Y, Wang X, Xue F. G-phase precipitation in duplex stainless steels after long-term thermal aging: a high-resolution transmission electron microscopy study. *Journal of Nuclear Materials*. 2014;452(1-3):382-388.

11. Chandra K, Singhal R, Kain V, Raja VS. Low temperature embrittlement of duplex stainless steel: Correlation between mechanical and electrochemical behavior. *Materials Science and Engineering: A*. 2010;527(16-17):3904-3912.

12. Iacoviello F, Casari F, Gialanella S. Effect of "475 °C embrittlement" on duplex stainless steels localized corrosion resistance. *Corrosion Science*. 2005;47(4):909-922.

13. Wang YQ, Li D, Sun L, Li N, Liu M, Shen W, et al. Pitting corrosion of thermally aged cast duplex stainless steel for primary coolant pipes of nuclear power plants. *Corrosion Engineering, Science and Technology*. 2017;52(6):447-452.

14. Frankel GS. Pitting corrosion of metals: a review of the critical factors. *Journal of the Electrochemical Society*. 1998;145(6):2186-2198.

15. Lv JL, Liang TX, Dong LM, Wang C. Influence of sensitization on microstructure and passive property of AISI 2205 duplex stainless steel. *Corrosion Science*. 2016;104:144-151.

16. Ryan MP, Williams DE, Chater RJ, Hutton BM, McPhail DS. Why stainless steel corrodes. *Nature*. 2002;415(6873):770-774.

17. Boucherit N, Goff AHL, Joiret S. Influence of Ni, Mo, and Cr on pitting corrosion of steels studied by raman spectroscopy. *Corrosion*. 1992;48(7):569-579.

18. Wang YQ, Li N, Yang B. Effect of ferrite on pitting corrosion of Fe20Cr9Ni cast austenite stainless steel for nuclear power plant pipe. *Corrosion Engineering, Science and Technology*. 2015;50(4):330-337.

19. Zhang LH, Zhang W, Jiang YM, Deng B, Sun DM, Li J. Influence of annealing treatment on the corrosion resistance of lean duplex stainless steel 2101. *Electrochimica Acta*. 2009;54(23):5387-5392.

20. Park CJ, Kwon HS. Effects of aging at 475 °C on corrosion properties of tungsten-containing duplex stainless steels. *Corrosion Science*. 2002;44(12):2817-2830.

21. Yi YS, Shoji T. Detection and evaluation of material degradation of thermally aged duplex stainless steels: electrochemical polarization test and AFM surface analysis. *Journal of Nuclear Materials*. 1996;231(1-2):20-28.

22. Park JS, Yoon YK. Evaluation of thermal aging embrittlement of duplex stainless steels by electrochemical method. *Scripta Metallurgica et Materialia*. 1995;32(8):1163-1168.

23. Berg HP. Corrosion mechanisms and their consequences for nuclear power plants with light water reactors. *Reliability and risk analysis: theory and applications.* 2009;2:57-68.

24. Chandra K, Kain V, Raja VS, Tewari R, Dey GK. Low temperature thermal ageing embrittlement of austenitic stainless steel welds and its electrochemical assessment. *Corrosion Science*. 2012;54:278-290.

25. Hättestrand M, Larsson P, Chai G, Nilsson JO, Odqvist J. Study of decomposition of ferrite in a duplex stainless steel cold worked and aged at 450 - 500 °C. *Materials Science and Engineering:A*. 2009;499(1):489-492.

26. Almanza E, Murr LE. A comparison of sensitization kinetics in 304 and 316 stainless steels. *Journal of Materials Science.* 2000;35(13):3181-3188.

27. Tavares SSM, Terra VF, Lima Neto P, Matos ER. Corrosion resistance evaluation of the UNS S31803 duplex stainless steels aged at low temperature (350 to 550°C) using DLEPR tests. *Journal of Materials Science.* 2005;40(15):4025-4028.

28. Ahn YS, Kim JM, Jeong BH. Effect of aging treatments and microstructural evolution on corrosion resistance of tungsten sbustitued 2205 duplex stainless steel. *Materials Science and Technology*. 2002;18(4):383-388.

29. Wang YQ, Yang B, Han J, Wu HC, Wang X. Effect of precipitated phases on the pitting corrosion of Z3CN20.09M cast duplex stainless steel. *Materials Transactions*. 2013;54(5):839-843.

30. Ilevbare GE, Burstein GT. Role of alloyed molybdenum in the inhibition of pitting corrosion in stainless steels. *Corrosion Science*. 2001;43(3):485-513.

31. Pardo A, Merino MC, Coy AE, Viejo F, Arrabal R, Matykina E. Pitting corrosion behaviour of austenitic stainless steels - combining effects of Mn and Mo additions. *Corrosion Science*. 2008;50(6):1796-1806.

32. Deng B, Jiang YM, Gong J, Zhong C, Gao J, Li J. Critical pitting and repassivation temperatures for duplex stainless steel in chloride solutions. *Electrochimica Acta.* 2008;53(16):5220-5225.

33. Lo KH, Kwok CT, Chan WK, Zeng D. Corrosion resistance of duplex stainless steel subjected to long-term annealing in the spinodal decomposition temperature range. *Corrosion Science*. 2012;55:267-271.